Available online at www.sciencedirect.com
ScienceDirect
Journal of Sound and Vibration 320 (2009) 84–100
JOURNAL OF SOUND AND VIBRATION
www.elsevier.com/locate/jsvi

Modal power flow analysis of a damaged plate

W.O. Wong*, X.Q. Wang, L. Cheng

Department of Mechanical Engineering, The Hong Kong Polytechnic University, Hung Hom, Kowloon, Hong Kong SAR

Received 27 March 2008; received in revised form 30 June 2008; accepted 13 July 2008
Handling Editor: J. Lam
Available online 27 August 2008

Abstract

Variation of the modal reactive power distribution of a damaged plate is analyzed. Large variation of local reactive power flow in or around the damage region of a plate under resonant vibration is related to the change of strain and kinetic energies in the damage region. Feasibility of damage identification based on the detection of this local variation of modal reactive power flow in a structure is studied. Compared with the damage identification techniques based on the determination of the active power flow in a damaged plate, the proposed method only requires data of a vibration mode shape of the structure and it is easier to apply in practice. Two common types of damage have been tested for identification, the first with a region of reduced stiffness in the plate while the second with a small hole in the plate. Numerical tests show that the proposed method is effective for both types of damage and the modal power flow is more sensitive to the change of plate stiffness than the strain mode shape in the test case.

1. Introduction

Detection of damage occurring in structures is an important topic in mechanical and structural engineering applications [1–3]. Identification of damage location is crucial for damage repair and control and there have been many techniques developed for damage identification and location in recent years [4–7]. One relatively new technique is based on the study of power flow or structural intensity (SI) in a vibrating structure. There are in general active and reactive powers presented in a vibrating structure. Active power is defined as the product of a generalized force with the in-phase component of a generalized velocity, where the velocity is in the same direction as the force. Forces and velocities in a vibrating structure will be exactly 90° out of phase if no damping and no energy dissipation such as sound radiation in the system is assumed. The product of the corresponding force and velocity terms is called the reactive power, which represents the amount of energy stored in the structure [8].

Li et al. [9] proposed the diagnosis of flaws in damaged beam structures using vibrational power flow. Khun et al. [10] showed that loosened bolt joints in plate assembly could be identified from the power flow pattern in the plates. Lee et al. [11] calculated the diversion of energy flow near crack tips of a vibrating plate using SI technique. They showed that the presence of a crack can be identified by the changes of the directions of SI

*Corresponding author. Tel.: +852 2766 6667; fax: +852 2365 4703.
E-mail address: mmwowong@polyu.edu.hk (W.O. Wong).

0022-460X/$ - see front matter © 2008 Elsevier Ltd. All rights reserved.
doi:10.1016/j.jsv.2008.07.004

vectors near the crack. In all these reported methods, however, the forced vibration data of an excited structure were required. Accordingly, it was the active power flow which was used for damage identification. There is no report found in the literature about the use of reactive power flow in a plate for damage identification.

The aim of this paper is to study the power flow and energy distribution of a vibration mode of a damaged plate. The power flow is shown to be of reactive nature in this case, and referred to as the modal power flow in the following. The outline of this paper is as follows. In Section 2, the modal power flow analysis of the damaged plate is performed, and the relation between the modal power flow and the modal energy distribution in the plate is derived. The modal power flow is proposed to locate damage sites in plate-like structures. In Section 3, some numerical simulations are demonstrated to analyze the identification capability of the proposed damage indicator. Finally, conclusions are drawn.

2. Modal power flow analysis of a damaged plate

From plate theory, the equation of motion of a thin vibrating plate may be written as

$$D\left(\frac{\partial^4 w}{\partial x^4}+2\frac{\partial^4 w}{\partial x^2\partial y^2}+\frac{\partial^4 w}{\partial y^4}\right)+\rho h\frac{\partial^2 w}{\partial t^2}=0 \tag{1}$$

where $D=Eh^3/12(1-v^2)$ is the flexural rigidity of the plate, E is the modulus of elasticity, v is the Poisson ratio, h is the thickness of the plate, and ρ is the material density.

Assuming the plate has a harmonic motion of frequency ω, its displacement may be written as

$$w(x,y;t)=W(x,y)\sin\,\omega t \tag{2}$$

where $W(x, y)$ is the vibration amplitude of the plate.

The strain distributions of the plate may be written as

$$\Psi_x(x,y)=\frac{\partial^2 W(x,y)}{\partial x^2},\quad \Psi_y(x,y)=\frac{\partial^2 W(x,y)}{\partial y^2},\quad \Psi_{xy}(x,y)=\frac{\partial^2 W(x,y)}{\partial x\partial y} \tag{3}$$

The instantaneous power flow at point (x, y) may be written as [12]

$$\vec{P}(x,y;t)=P_x(x,y;t)\vec{i}+P_y(x,y;t)\vec{j} \tag{4}$$

where

$$P_x(x,y;t)=D\left[\frac{\partial(\nabla^2 w)}{\partial x}\dot{w}-\left(\frac{\partial^2 w}{\partial x^2}+v\frac{\partial^2 w}{\partial y^2}\right)\frac{\partial\dot{w}}{\partial x}-(1-v)\frac{\partial^2 w}{\partial x\partial y}\frac{\partial\dot{w}}{\partial y}\right] \tag{5}$$

and

$$P_y(x,y;t)=D\left[\frac{\partial(\nabla^2 w)}{\partial y}\dot{w}-\left(\frac{\partial^2 w}{\partial y^2}+v\frac{\partial^2 w}{\partial x^2}\right)\frac{\partial\dot{w}}{\partial y}-(1-v)\frac{\partial^2 w}{\partial y\partial x}\frac{\partial\dot{w}}{\partial x}\right] \tag{6}$$

2.1. Relationship between power flow and energy distributions of a vibrating plate

Eq. (5) may be rewritten using Eqs. (2) and (3) as

$$\begin{aligned}P_x(x,y;t)&=D\left[\frac{\partial(\nabla^2 w)}{\partial x}\dot{w}-\left(\frac{\partial^2 w}{\partial x^2}+v\frac{\partial^2 w}{\partial y^2}\right)\frac{\partial\dot{w}}{\partial x}-(1-v)\frac{\partial^2 w}{\partial x\partial y}\frac{\partial\dot{w}}{\partial y}\right]\\&=\frac{1}{2}\omega D\left[\frac{\partial(\Psi_x+\Psi_y)}{\partial x}W-(\Psi_x+v\Psi_y)\frac{\partial W}{\partial x}-(1-v)\Psi_{xy}\frac{\partial W}{\partial y}\right]\sin\,2\omega t\\&=P_{x\_\max}\sin\,2\omega t\end{aligned} \tag{7a}$$

where

$$P_{x\_\max} = \frac{1}{2}\omega D\left[\frac{\partial(\Psi_x + \Psi_y)}{\partial x} W - (\Psi_x + v\Psi_y)\frac{\partial W}{\partial x} - (1-v)\Psi_{xy}\frac{\partial W}{\partial y}\right] \tag{7b}$$

Eq. (6) may be rewritten using Eqs. (2) and (3) as

$$\begin{aligned} P_y(x,y;t) &= D\left[\frac{\partial(\nabla^2 w)}{\partial y}\dot{w} - \left(\frac{\partial^2 w}{\partial y^2} + v\frac{\partial^2 w}{\partial x^2}\right)\frac{\partial \dot{w}}{\partial y} - (1-v)\frac{\partial^2 w}{\partial y \partial x}\frac{\partial \dot{w}}{\partial x}\right] \\ &= \frac{1}{2}\omega D\left[\frac{\partial(\Psi_x + \partial\Psi_y)}{\partial y} W - (\Psi_y + v\Psi_x)\frac{\partial W}{\partial y} - (1-v)\Psi_{xy}\frac{\partial W}{\partial x}\right]\sin 2\omega t \\ &= P_{y\_\max}\sin 2\omega t \end{aligned} \tag{8a}$$

where

$$P_{y\_\max} = \frac{1}{2}\omega D\left[\frac{\partial(\Psi_x + \Psi_y)}{\partial y} W - (\Psi_y + v\Psi_x)\frac{\partial W}{\partial y} - (1-v)\Psi_{xy}\frac{\partial W}{\partial x}\right] \tag{8b}$$

The power gradients may be written as

$$\begin{aligned} \frac{\partial P_x}{\partial x} = \frac{1}{2}\omega D\Bigg[&\frac{\partial^2(\nabla^2 W)}{\partial x^2} W + \frac{\partial(\nabla^2 W)}{\partial x}\frac{\partial W}{\partial x} - \left(\frac{\partial^3 W}{\partial x^3} + v\frac{\partial^3 W}{\partial x \partial y^2}\right)\frac{\partial W}{\partial x} \\ &- \left(\frac{\partial^2 W}{\partial x^2} + v\frac{\partial^2 W}{\partial y^2}\right)\frac{\partial^2 W}{\partial x^2} - (1-v)\left(\frac{\partial^2 W}{\partial x \partial y}\frac{\partial^2 W}{\partial y \partial x} + \frac{\partial^3 W}{\partial x^2 \partial y}\frac{\partial W}{\partial y}\right)\Bigg]\sin 2\omega t \end{aligned} \tag{9}$$

and

$$\begin{aligned} \frac{\partial P_y}{\partial y} = \frac{1}{2}\omega D\Bigg[&\frac{\partial^2(\nabla^2 W)}{\partial y^2} W + \frac{\partial(\nabla^2 w)}{\partial y}\frac{\partial W}{\partial y} - \left(\frac{\partial^3 W}{\partial y^3} + v\frac{\partial^3 W}{\partial y \partial x^2}\right)\frac{\partial W}{\partial y} \\ &- \left(\frac{\partial^2 W}{\partial y^2} + v\frac{\partial^2 W}{\partial x^2}\right)\frac{\partial^2 W}{\partial y^2} - (1-v)\left(\frac{\partial^2 W}{\partial x \partial y}\frac{\partial^2 W}{\partial y \partial x} + \frac{\partial^3 W}{\partial y^2 \partial x}\frac{\partial W}{\partial x}\right)\Bigg]\sin 2\omega t \end{aligned} \tag{10}$$

The power flow $\vec{P}(x,y;t)$ can be related to the instantaneous energy stored in the plate in the following. The distribution of the instantaneous kinetic energy of the plate may be written as

$$\begin{aligned} T &= \tfrac{1}{2}\rho h\omega^2 W^2 \cos^2\omega t \\ &= T_{\max}\cos^2\omega t \end{aligned} \tag{11}$$

where

$$T_{\max} = \tfrac{1}{2}\rho h\omega^2 W^2 \tag{12}$$

The distribution of the instantaneous strain energy of the plate may be written as

$$\begin{aligned} U &= \frac{1}{2}\omega D\left[\left(\frac{\partial^2 W}{\partial x^2}\right)^2 + \left(\frac{\partial^2 W}{\partial y^2}\right)^2 + 2v\frac{\partial^2 W}{\partial x^2}\frac{\partial^2 W}{\partial y^2} + 2(1-v)\left(\frac{\partial^2 W}{\partial x \partial y}\right)^2\right]\sin^2\omega t \\ &= U_{\max}\sin^2\omega t \end{aligned} \tag{13}$$

where

$$U_{\max} = \frac{1}{2}\omega D\left[\left(\frac{\partial^2 W}{\partial x^2}\right)^2 + \left(\frac{\partial^2 W}{\partial y^2}\right)^2 + 2v\frac{\partial^2 W}{\partial x^2}\frac{\partial^2 W}{\partial y^2} + 2(1-v)\left(\frac{\partial^2 W}{\partial x \partial y}\right)^2\right] \tag{14}$$

The instantaneous energy and distributions in the plate are written, respectively, as

$$\begin{aligned} E &= T_{\max}\cos^2\omega t + U_{\max}\sin^2\omega t \\ &= \tfrac{1}{2}(T_{\max} + U_{\max}) + \tfrac{1}{2}(T_{\max} - U_{\max})\cos 2\omega t \end{aligned} \tag{15}$$

and

$$\frac{\partial E}{\partial t} = \omega(T_{\max} - U_{\max}) \sin 2\omega t \tag{16}$$

Using Eqs. (9) and (10), the sum of the power flow gradients can be written as

$$\begin{aligned}\frac{\partial P_x}{\partial x} + \frac{\partial P_y}{\partial y} &= \frac{1}{2}\omega D\left[\frac{\partial^2(\nabla^2 W)}{\partial x^2} W + \frac{\partial(\nabla^2 W)}{\partial x}\frac{\partial W}{\partial x} + \frac{\partial^2(\nabla^2 W)}{\partial y^2} W + \frac{\partial(\nabla^2 W)}{\partial y}\frac{\partial W}{\partial y} - \left(\frac{\partial^2 W}{\partial y^2} + \nu\frac{\partial^2 W}{\partial x^2}\right)\frac{\partial^2 W}{\partial y^2}\right.\\ &\quad \left. - \left(\frac{\partial^2 W}{\partial x^2} + \nu\frac{\partial^2 W}{\partial y^2}\right)\frac{\partial^2 W}{\partial x^2} - (1-\nu)\left(\frac{\partial^2 W}{\partial x \partial y}\frac{\partial^2 W}{\partial y \partial x} + \frac{\partial^2 W}{\partial y \partial x}\frac{\partial^2 W}{\partial x \partial y}\right)\right] \sin 2\omega t\\ &= \frac{1}{2}\omega D W\left[\frac{\partial^4 W}{\partial x^4} + 2\left(\frac{\partial^2 W}{\partial x^2}\frac{\partial^2 W}{\partial y^2}\right) + \frac{\partial^4 W}{\partial y^4}\right] \sin 2\omega t\\ &\quad - \frac{1}{2}\omega D\left[\left(\frac{\partial^2 W}{\partial x^2}\right)^2 + \left(\frac{\partial^2 W}{\partial y^2}\right)^2 + 2\nu\frac{\partial^2 W}{\partial x^2}\frac{\partial^2 W}{\partial y^2} + 2(1-\nu)\left(\frac{\partial^2 W}{\partial x \partial y}\right)^2\right] \sin 2\omega t\end{aligned} \tag{17}$$

Eq. (1) may be rewritten using Eq. (2) as

$$D\left[\frac{\partial^4 W}{\partial x^4} + 2\left(\frac{\partial^2 W}{\partial x^2}\frac{\partial^2 W}{\partial y^2}\right) + \frac{\partial^4 W}{\partial y^4}\right] = \rho h \omega^2 W \tag{18}$$

Eq. (17) can be rewritten using Eq. (18) as

$$\begin{aligned}\frac{\partial P_x}{\partial x} + \frac{\partial P_y}{\partial y} = \frac{1}{2}\omega\left\{\rho h \omega^2 W^2 - D\left[\left(\frac{\partial^2 W}{\partial x^2}\right)^2 + \left(\frac{\partial^2 W}{\partial y^2}\right)^2\right.\right.\\ \left.\left. + 2\nu\frac{\partial^2 W}{\partial x^2}\frac{\partial^2 W}{\partial y^2} + 2(1-\nu)\left(\frac{\partial^2 W}{\partial x \partial y}\right)^2\right]\right\} \sin 2\omega t\end{aligned} \tag{19}$$

Using Eqs. (12), (14) and (16), the instantaneous energy balance at a point (x, y) of the plate may be written as

$$\frac{\partial P_x}{\partial x} + \frac{\partial P_y}{\partial y} = \frac{\partial E}{\partial t} \tag{20}$$

The net power flow out of a region $x_1 \leqslant x \leqslant x_2$ and $y_1 \leqslant y \leqslant y_2$ can be obtained by integrating the above equation along x-direction from x_1 to x_2 and along y direction from y_1 to y_2 and the result may be written as

$$\int_{y_1}^{y_2} [P_x(x_2) - P_x(x_1)]\,\mathrm{d}y + \int_{x_1}^{x_2} [P_y(y_2) - P_y(y_1)]\,\mathrm{d}x = \omega \int_{y_1}^{y_2}\int_{x_1}^{x_2} (T_{\max} - U_{\max})\,\mathrm{d}x\,\mathrm{d}y \sin 2\omega t \tag{21}$$

This energy flow and balance in a region of the plate is illustrated in Fig. 1.

Using Eqs. (7), (8), (16) and (20), we may write

$$\frac{\partial P_{x\_\max}}{\partial x} + \frac{\partial P_{y\_\max}}{\partial y} = \omega(T_{\max} - U_{\max}) \tag{22}$$

Eq. (22) shows that the sum of power flow gradients is proportional to the Lagrangian density $(T_{\max} - U_{\max})$ of the plate.

2.2. Modal power flow of a plate

Since damping is neglected in the present analysis, the force and moment terms has no in-phase component of the corresponding velocity terms in the calculation of the power flow of a vibration mode of the plate. Therefore, the power flow of a vibration mode of the plate is the reactive power associated with that particular mode and it is termed as the modal power flow in the following analysis.

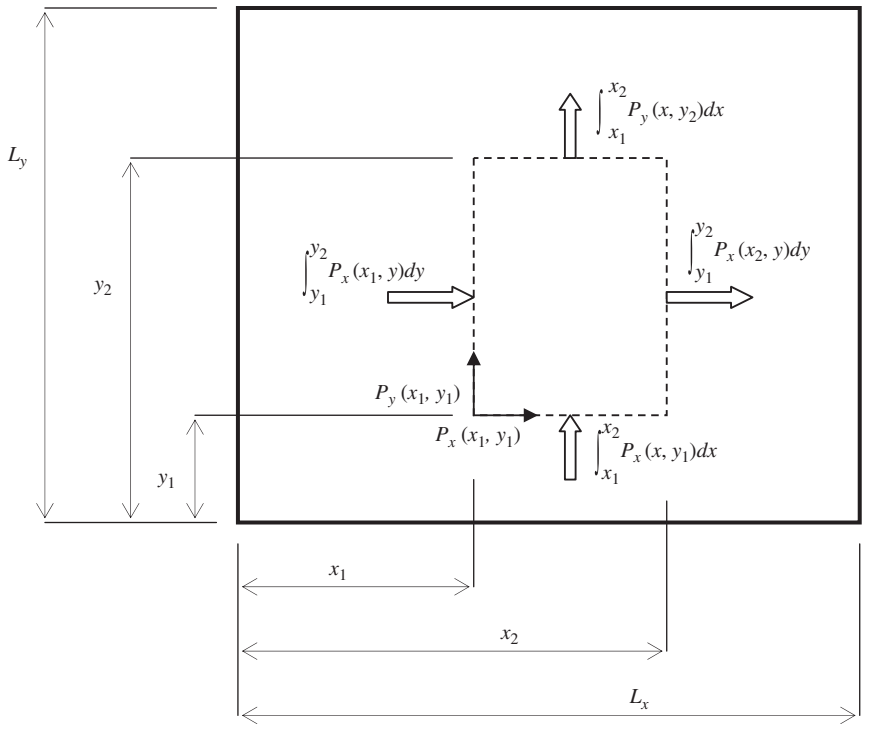

Fig. 1. Illustration of the power flow in and out of a region (as shown by the hollow arrows) in a vibrating plate.

Using Eqs. (4)–(6), the reactive power flow at the mnth mode where $m, n = 1, 2, 3\ldots$, may be defined as

$$\vec{P}_{mn}(x, y; t) = P_{mn\_x}(x, y) \sin 2\omega_{mn} t\vec{i} + P_{mn\_y}(x, y) \sin 2\omega_{mn} t\vec{j} \tag{23}$$

where

$$P_{mn\_x}(x, y) = D\omega_{mn}\left[\frac{\partial(\nabla^2 W_{mn})}{\partial x} W_{mn} - \left(\frac{\partial^2 W_{mn}}{\partial x^2} + v\frac{\partial^2 W_{mn}}{\partial y^2}\right)\frac{\partial W_{mn}}{\partial x} - (1-v)\frac{\partial^2 W_{mn}}{\partial x \partial y}\frac{\partial W_{mn}}{\partial y}\right] \tag{24}$$

and

$$P_{mn\_y}(x, y) = D\omega_{mn}\left[\frac{\partial(\nabla^2 W_{mn})}{\partial y} W_{mn} - \left(\frac{\partial^2 W_{mn}}{\partial y^2} + v\frac{\partial^2 W_{mn}}{\partial x^2}\right)\frac{\partial W_{mn}}{\partial y} - (1-v)\frac{\partial^2 W_{mn}}{\partial y \partial x}\frac{\partial W_{mn}}{\partial x}\right] \tag{25}$$

where ω_{mn} and W_{mn} are the natural frequency and mode shape of the mnth vibration mode of the plate, respectively. From Eq. (20), the modal power flow can be related to the modal energy distribution of the plate as

$$\frac{\partial P_{mn\_x}}{\partial x} + \frac{\partial P_{mn\_y}}{\partial y} = \omega_{mn}(T_{mn\_\max} - U_{mn\_\max}) \tag{26}$$

where

$$T_{mn\_\max} = \tfrac{1}{2}\rho h \omega_{mn}^2 W_{mn}^2 \tag{27}$$

and

$$U_{mn\_\max} = \frac{1}{2}\omega_{mn} D\left[\left(\frac{\partial^2 W_{mn}}{\partial x^2}\right)^2 + \left(\frac{\partial^2 W_{mn}}{\partial y^2}\right)^2 + 2v\frac{\partial^2 W_{mn}}{\partial x^2}\frac{\partial^2 W_{mn}}{\partial y^2} + 2(1-v)\left(\frac{\partial^2 W_{mn}}{\partial x \partial y}\right)^2\right] \tag{28}$$

2.3. Damage identification from the modal power flow of a plate

This part deals with the damage identification in a plate using the information about modal power flow. The basic concept is that a localized loss of stiffness will produce a curvature increase at the same location [2]. If no change of mass in the damage region is assumed, this local change of curvature would induce a local change of bending strains [5] and strain energy distribution [6] around the damage region resulting in the change of the gradients of power flow around the region as depicted by Eq. (26). This change of modal power flow may be more sensitive to the damage as it is a higher order derivative of the mode shape than the strain distribution of the plate [13].

The modal power flow vector field may be rewritten as

$$\frac{\vec{P}_{mn}(x,y;t)}{\omega_{mn}D} = [\tilde{P}_{mn\_x}(x,y)\vec{i} + \tilde{P}_{mn\_y}(x,y)\vec{j}]\sin 2\omega_{mn}t \tag{29}$$

where

$$\tilde{P}_{mn\_x}(x,y) = \left[\frac{\partial(\nabla^2 W_{mn})}{\partial x}W_{mn} - \left(\frac{\partial^2 W_{mn}}{\partial x^2} + v\frac{\partial^2 W_{mn}}{\partial y^2}\right)\frac{\partial W_{mn}}{\partial x} - (1-v)\frac{\partial^2 W_{mn}}{\partial x \partial y}\frac{\partial W_{mn}}{\partial y}\right] \tag{30}$$

and

$$\tilde{P}_{mn\_y}(x,y) = \left[\frac{\partial(\nabla^2 W_{mn})}{\partial y}W_{mn} - \left(\frac{\partial^2 W_{mn}}{\partial y^2} + v\frac{\partial^2 W_{mn}}{\partial x^2}\right)\frac{\partial W_{mn}}{\partial y} - (1-v)\frac{\partial^2 W_{mn}}{\partial y \partial x}\frac{\partial W_{mn}}{\partial x}\right] \tag{31}$$

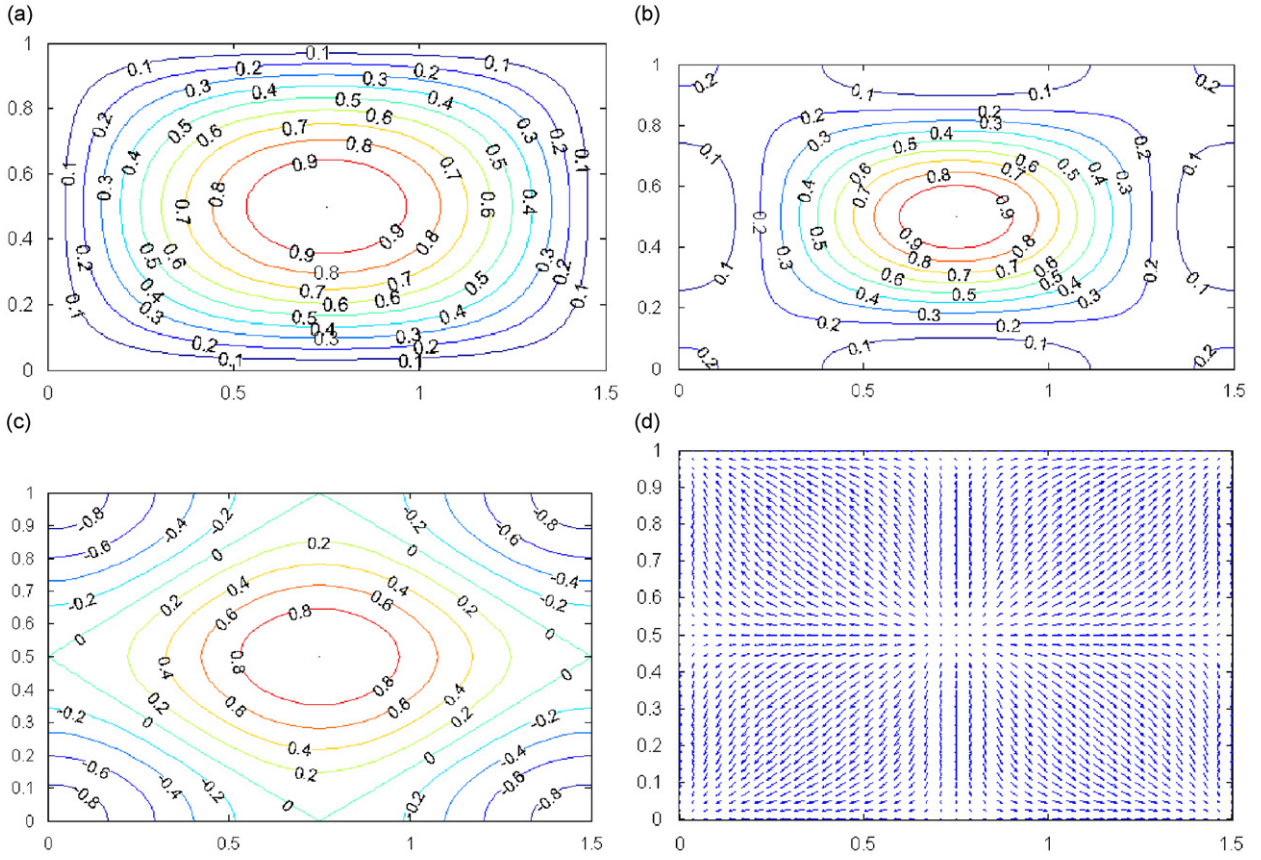

Fig. 2. (a) Contours of vibration mode shape W_{11} of a simply supported rectangular plate, (b) contours of the stationary modal energy ($T_{11\_max} + V_{11\_max}$), (c) contour of the time varying modal energy ($T_{11\_max} - V_{11\_max}$) and (d) modal power flow $\vec{P}_{11}(x,y)/D\omega_{11}$ (illustrated by the arrows).

The vector field $\vec{P}_{mn}(x,y)/\omega_{mn}D = \tilde{P}_{mn\_x}\vec{i} + \tilde{P}_{mn\_y}\vec{j}$ is proposed to be used for damage identification and location in plate-like structures. The advantage of using this term is that both the modal power flow components $\tilde{P}_{mn\_x}$ and $\tilde{P}_{mn\_y}$ can be derived by the mode shape data which can be obtained with a standard modal testing procedure [14].

3. Simulation analyses

Two common types of damage are considered in the following analysis in plate vibration. The first with a region of reduced stiffness in the plate while the second with a small hole in the plate. The vibration modes and hence the modal power flow of a simply supported rectangular plate with the first type of damage are calculated with a self-developed *Matlab* program based on the Rayleigh–Ritz method [5,15] while those of the second type of damage are calculated with the commercial finite element software *Patran*. Changes of modal energy distributions and power flow due to these two types of damage in a plate are compared and discussed in the following sections. Modal power flow and modal energy distributions are calculated according to Eqs. (24), (25), (27) and (28).

3.1. Simulation of the modal power flow in a plate

A simply supported rectangular plate of size $1.5 \times 1 \times 0.01\,\mathrm{m}^3$ is used in the simulation. In applying the Rayleigh–Ritz method, the rth mode shape function of the plate is expressed in a series written as [5,15]

$$W_r(x,y) = \sum_{i=1}^{p}\sum_{j=1}^{q} c_{r,ij}\varphi_i(x)\eta_j(y) \tag{32}$$

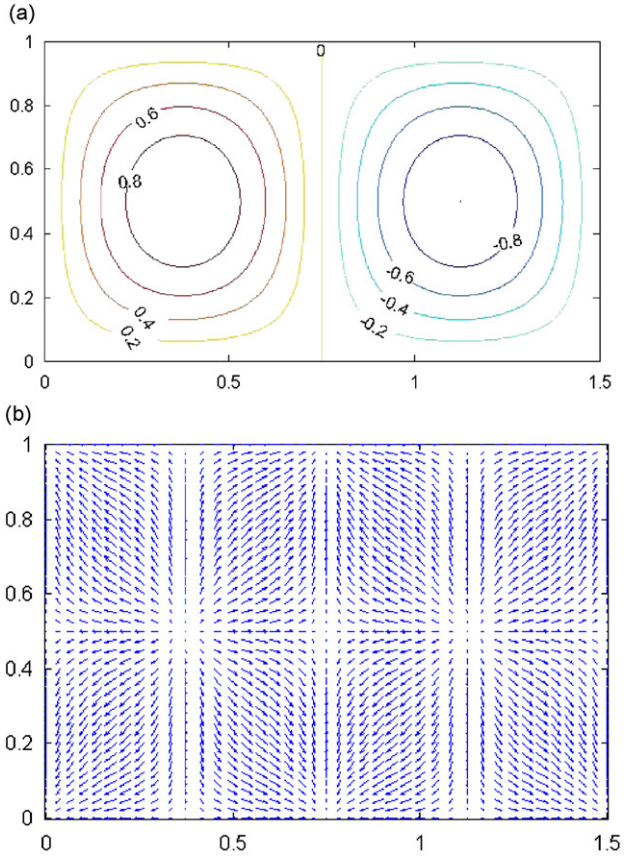

Fig. 3. (a) Contours of vibration mode shape W_{21} of a simply supported rectangular plate and (b) modal power flow $\vec{P}_{21}(x,y)/D\omega_{21}$ (illustrated by the arrows).

where $\varphi_i(x)$ and $\eta_j(y)$ are appropriate admissible functions, $c_{r,ij}$ the unknown coefficients. $p = q = 30$ is applied in the calculation of the mode shape functions.

Contour plots of the calculated mode shape functions and modal energy distributions are generated and displayed by using the CONTOUR function in Matlab. Fig. 2(a) shows the contours of the vibration mode W_{11} of the plate. Modal energy distributions of the plate are calculated according to Eqs. (12) and (14). Fig. 2(b) and (c) show the contours of the time-invariant modal energy distribution $T_{11\_max} + V_{11\_max}$ and the Lagrangian density distribution $T_{11\_max} - V_{11\_max}$, respectively. It should be noted that the modal power flow is proportional to the gradient of the Lagrangian density distribution; hence, the modal power flow would be more sensitive to a disturbance to the plate than the modal energy distribution. Fig. 2(d) shows the vector field of the modal power flow $\vec{P}_{11}/D\omega_{11}$ of the intact plate. Fig. 3(a) and (b) show the contours of the vibration mode W_{21} and the modal power flow $\vec{P}_{21}/D\omega_{21}$, respectively. It is observed that power flow is smallest at the anti-nodes and the corners and power radiates in and out from the anti-nodes to the edges and the nodal line. Fig. 4(a) and (b) show the contours of the vibration mode W_{31} and the modal power flow $\vec{P}_{31}/D\omega_{31}$,

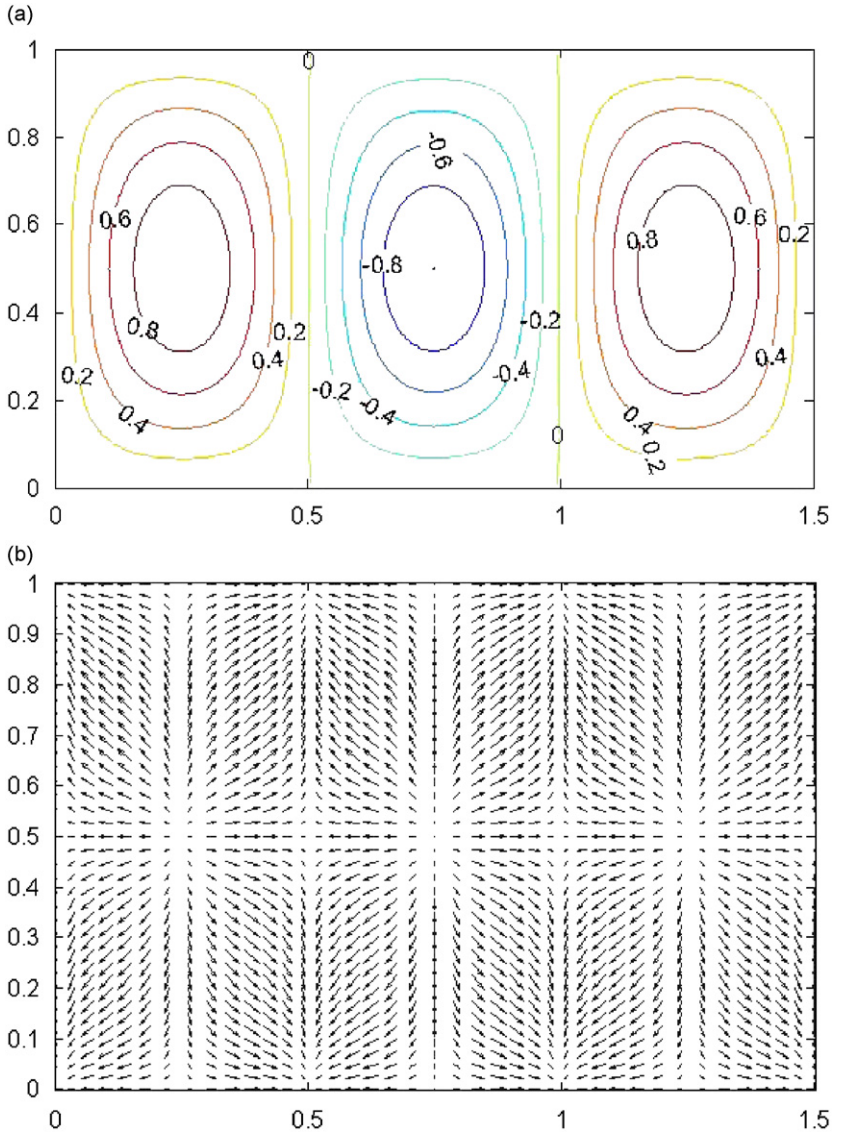

Fig. 4. (a) Contours of vibration mode shape W_{31} of a simply supported rectangular plate and (b) modal power flow $\vec{P}_{31}(x,y)/D\omega_{31}$ (illustrated by the arrows).

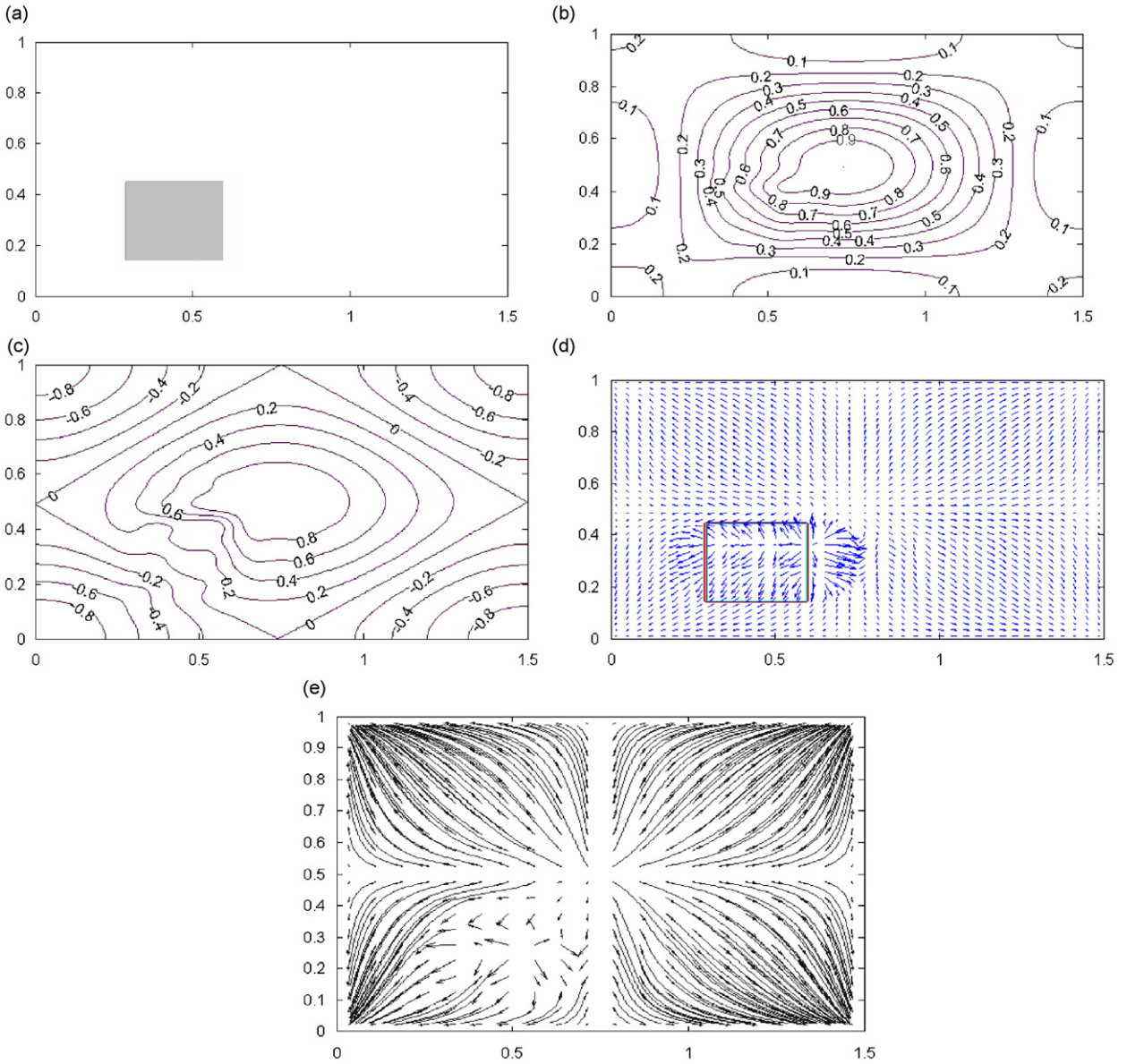

Fig. 5. (a) A simply supported rectangular plate with a damaged (shaded) region of 20% *EI* reduction, (b) contours of the stationary modal energy ($T_{11\_max}+V_{11\_max}$), (c) contour of the time-varying modal energy ($T_{11\_max}-V_{11\_max}$), (d) modal power flow ${}_{11}(x,y)/D\omega_{11}$ (illustrated by the arrows), and (e) streamline representation of the modal power flow $\vec{P}_{11}(x,y)/D\omega_{11}$ of the simply supported rectangular plate.

respectively. Similar to the previous case, power flow is smallest at the anti-nodes and the corners and power radiates in and out from the anti-nodes to the edges and the nodal line.

3.2. Change of modal power flow in a damaged plate

Fig. 5(a) illustrates the presence of a region, $0.3>x>0.6$ and $0.15>y>0.45$, with stiffness reduction of 20% in the plate. Fig. 5(b) and (c) show the time-invariant modal energy distribution $T_{11\_max}+V_{11\_max}$ and the Lagrangian density distribution $T_{11\_max}-V_{11\_max}$, respectively. It is observed that the modal energy distribution $T_{11\_max}+V_{11\_max}$ increases whilst the Lagrangian density distribution decreases in the damage

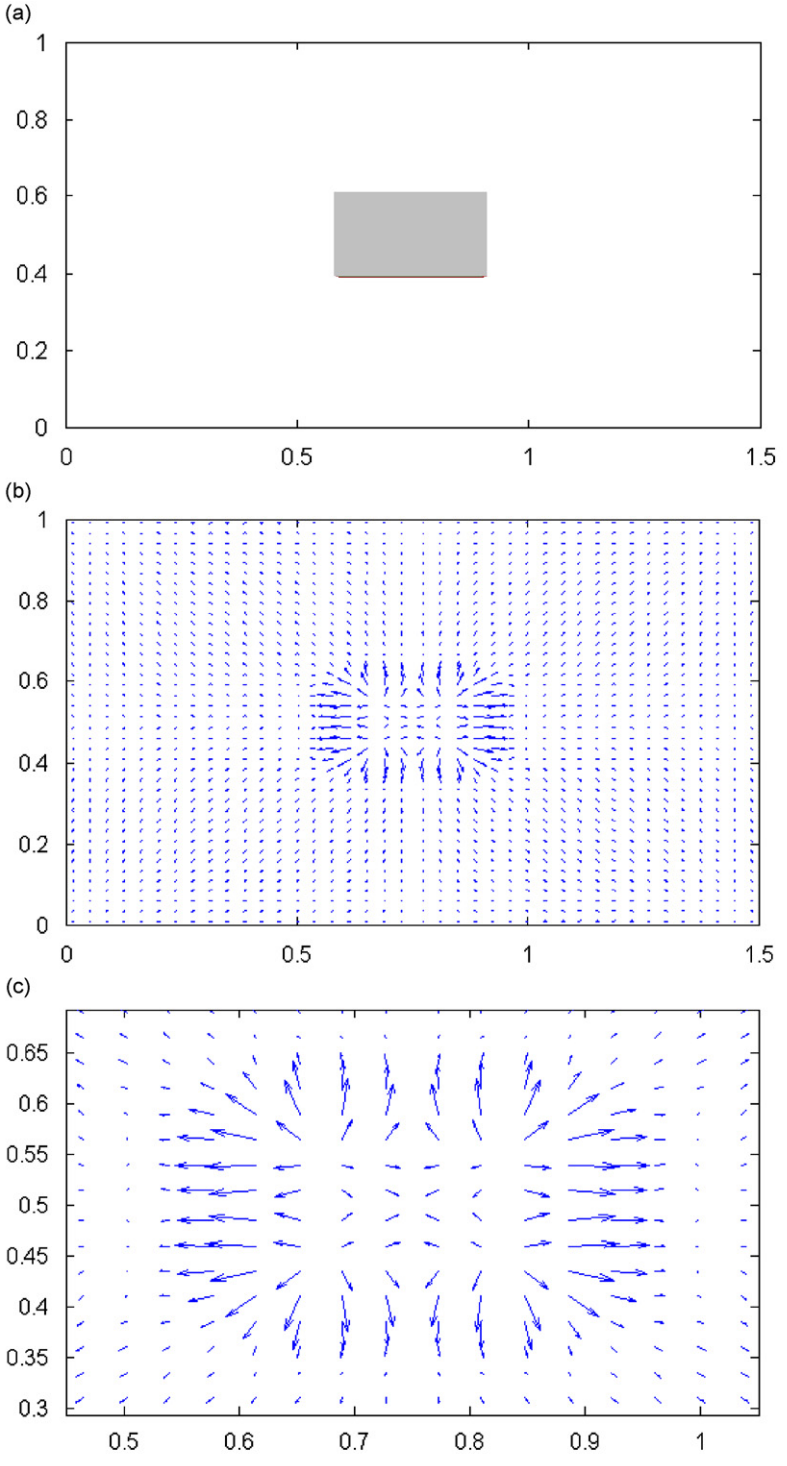

Fig. 6. (a) A simply supported plate with a damaged (shaded) region of 20% *EI* reduction, (b) modal power flow $\vec{P}_{11}(x,y)/D\omega_{11}$ (illustrated by the arrows) and (c) modal power flow in and around the damage region of the plate.

region. These effects would be a result of the increase of strain energy in the damage region as pointed out in Section 2.3. Fig. 5(d) is a vector plot of the modal power flow in the damaged plate. Significant changes in amplitude and direction of the modal power flow can be observed in and around the damage region. These changes are consistent with the prediction as depicted by Eq. (26). Obviously, the modal power flow distribution is a local parameter sensitive to damage. Fig. 5(e) is a plot of the modal power flow using the streamline representation [16,17] in the damaged plate. The streamlines around the damage region are discontinued because of the big changes of modal power flow in and around the damage region.

In order to investigate the identification capability of the proposed damage indicator, the vector plots of the modal power flow $\vec{P}_{mn}/\omega_{mn}D$ for damage occurring at a vibration anti-node and node of the structure are calculated and plotted in Figs. 6–8. Fig. 6(a) illustrates the presence of a damage region, $0.6>x>0.9$ and $0.4>y>0.6$, with stiffness reduction of 20% in the plate. Fig. 6(b) shows the modal power flow in the

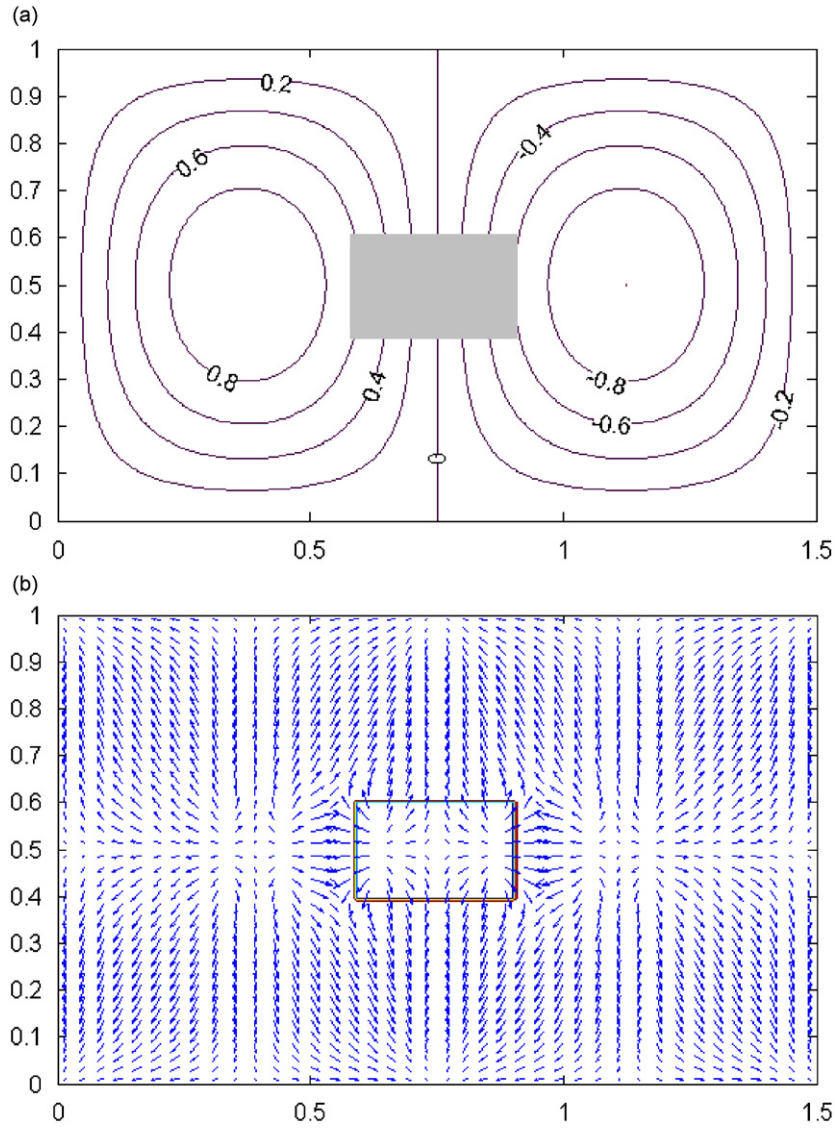

Fig. 7. (a) Contours of vibration mode shape W_{21} of the damaged plate in Fig. 6 and (b) modal power flow $\vec{P}_{21}(x,y)/D\omega_{21}$ (illustrated by the arrows).

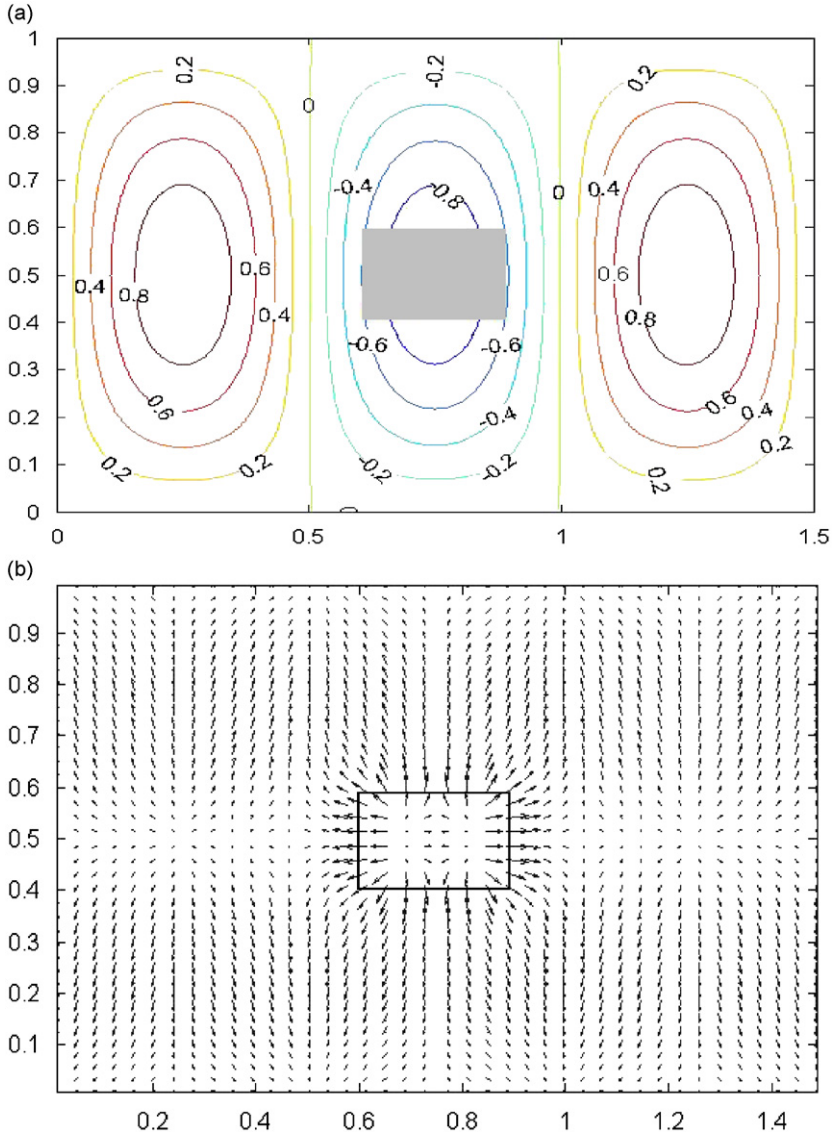

Fig. 8. (a) Contours of vibration mode shape W_{31} of the damaged plate in Fig. 6 and (b) modal power flow $\vec{P}_{31}(x,y)/D\omega_{31}$ (illustrated by the arrows).

damaged plate. Fig. 6(c) shows a close up of the modal power flow $\vec{P}_{11}/D\omega_{11}$, around the damage region for clarity. Similar to the previous case, significant changes in amplitude and direction of the modal power flow can be observed in and around the damage region. Fig. 7(a) and (b) show the contours of the second vibration mode W_{21} and the modal power flow $\vec{P}_{21}/D\omega_{21}$, respectively. Comparing Fig. 3(b) with Fig. 7(b), it is found that the modal power flow exhibits a big change in both the magnitude and direction even when the damage region is located at a nodal line of the vibration mode. Fig. 8(a) and (b) show the contours of the vibration mode W_{31} and the modal power flow $\vec{P}_{31}/D\omega_{31}$, respectively. Comparing Fig. 4(b) with Fig. 8(b), big changes in both the magnitude and direction of the modal power flow in and around the damaged region is observed. Streamline representations of modal power flow of both the intact and damaged plates are shown in Figs. 9(a)–(f). The streamlines in Fig. 9(a), (c) and (e) for the intact plate are continuous but those in Fig. 9(b) (d) and (f) for the damaged plate are not in the damaged region because of the big changes of modal power flow in that region.

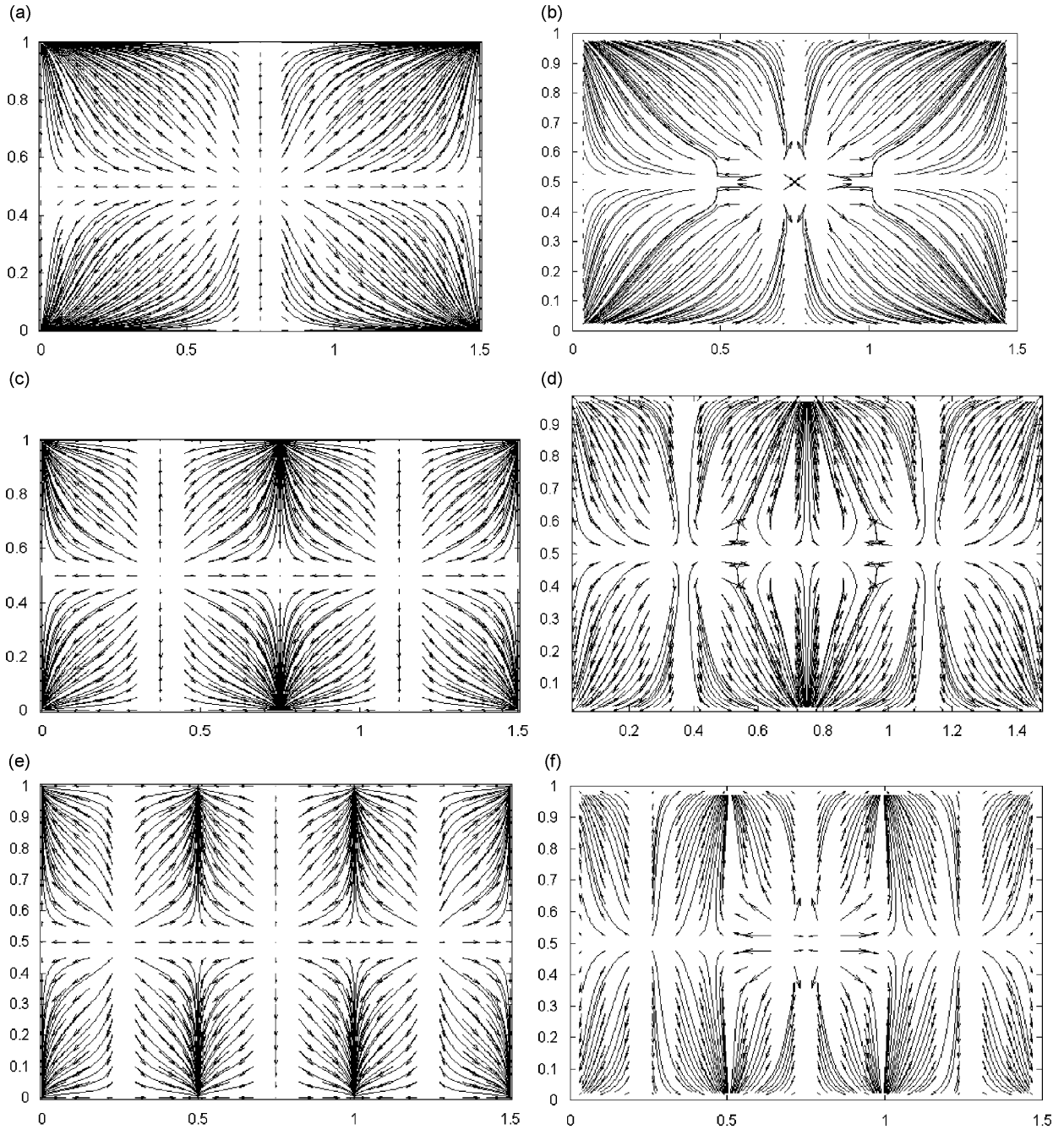

Fig. 9. (a) Streamline representation of the modal power flow $\vec{P}_{11}(x,y)/D\omega_{11}$ of the simply supported rectangular plate, (b) streamline representation of the modal power flow $\vec{P}_{11}(x,y)/D\omega_{11}$ of the simply supported damaged rectangular plate in Fig. 6a, (c) streamline representation of the modal power flow $\vec{P}_{21}(x,y)/D\omega_{21}$ of the simply supported rectangular plate, (d) streamline representation of the modal power flow $\vec{P}_{21}(x,y)/D\omega_{21}$ of the simply supported damaged rectangular plate in Fig. 6a, (e) streamline representation of the modal power flow $\vec{P}_{31}(x,y)/D\omega_{31}$ of the simply supported rectangular plate and (f) streamline representation of the modal power flow $\vec{P}_{31}(x,y)/D\omega_{31}$ of the simply supported damaged rectangular plate in Fig. 6a.

3.2.1. Sensitivity of parameters, $\varepsilon_{mn\_x}(x, y)$ and $P_{mn\_x}(x, y)$

Fig. 10(a) illustrates the presence of a region, $0.3>x>0.6$ and $0.1>y>0.3$, with stiffness reduction of 5% in the plate. Fig. 10(b) is a plot of the distribution of modal strain along x-direction $\varepsilon_{11\_x}(x, y)$. Contours of the

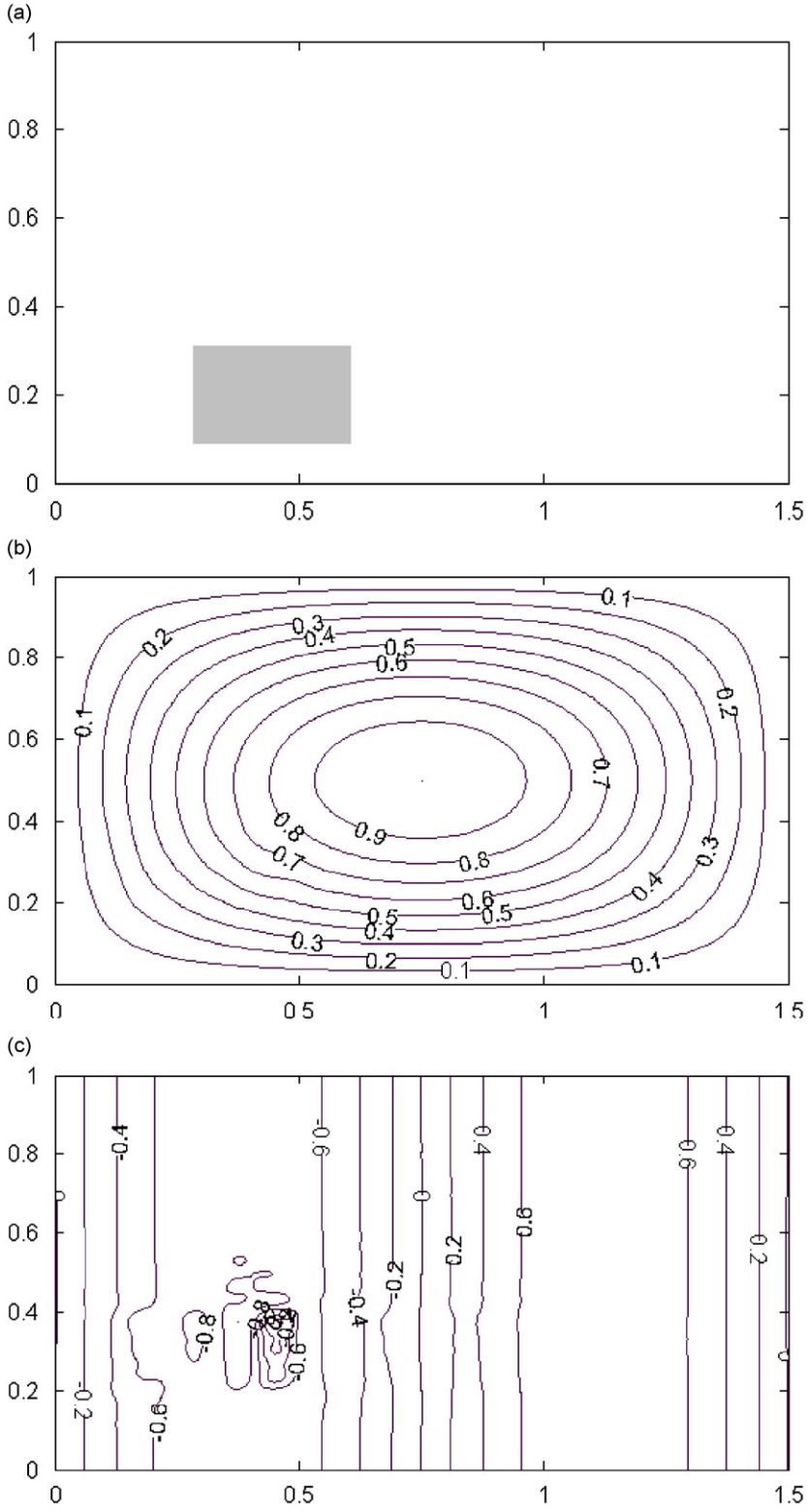

Fig. 10. (a) A rectangular plate with a damaged (shaded) region of *EI* reduction of 5%, (b) contour of the normalized strain mode shape ε_{11_x} of the damaged plate and (c) contour of the normalized modal power flow $\vec{P}_{11}(x,y)/D\omega_{11}$ of the damaged plate.

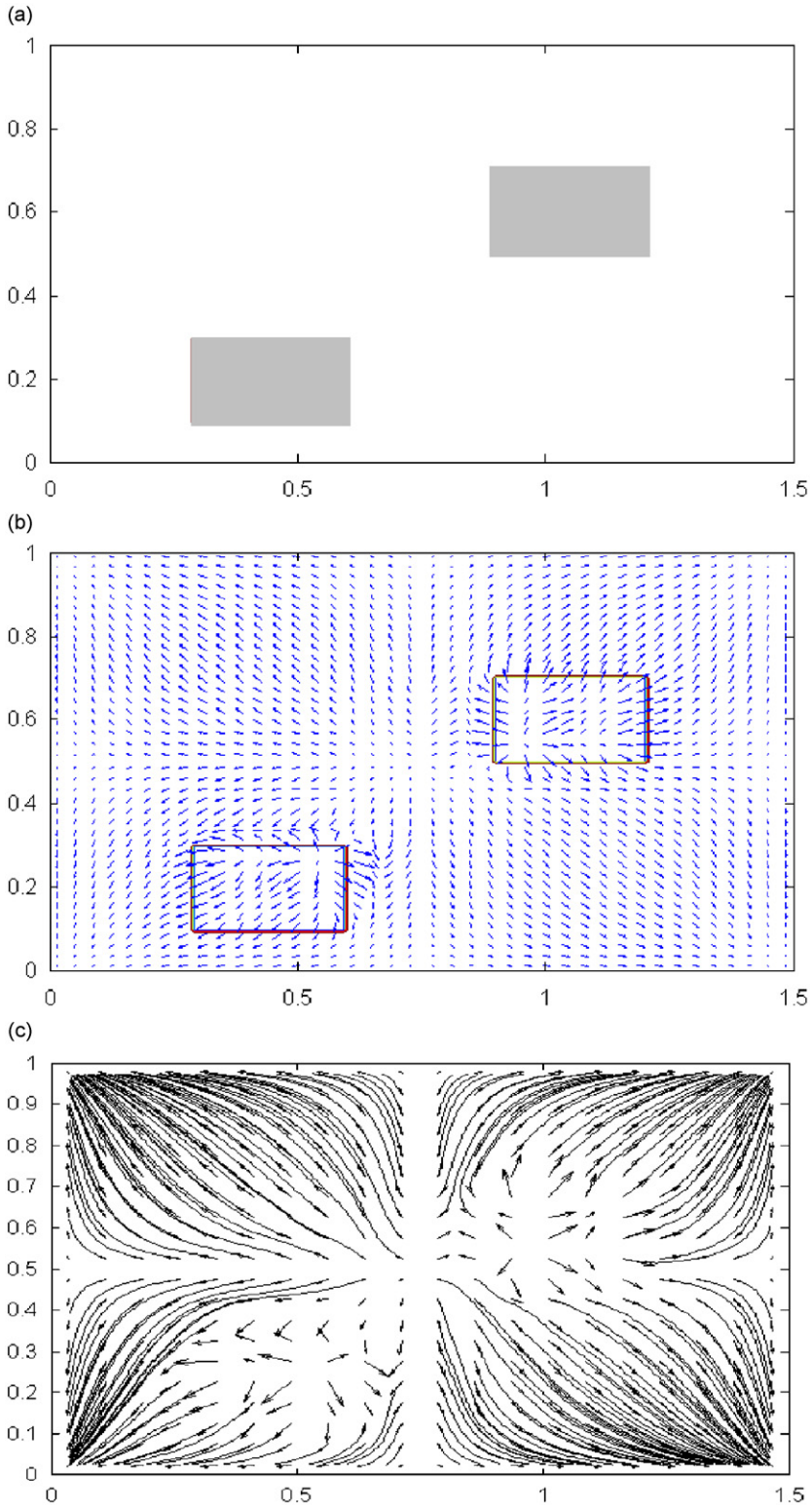

Fig. 11. (a) A rectangular plate with two damage regions (shaded) of *EI* reduction of 20% in the lower region and *EI* reduction of 10% in the upper region, (b) modal power flow $\vec{P}_{11}(x,y)/D\omega_{11}$ of the damaged plate. The damage regions are marked by two rectangles, and (c) streamline representation of the modal power flow $\vec{P}_{11}(x,y)/D\omega_{11}$ of the simply supported rectangular plate.

modal power flow component along x-direction $P_{11\_x}(x, y)$ is plotted in Fig. 10(c) for comparison. It can be observed that the strain distribution shows little change in the damage region while the modal power flow component has very large variations in the damage region.

3.2.2. Location of multiple damage in the structure

Fig. 11(a) illustrates the presence of two damage regions; one is $0.3>x>0.6$ and $0.1>y>0.3$, with plate stiffness reduction of 20% and another one is $0.9>x>1.2$ and $0.1>y>0.3$, with plate stiffness reduction of 10%. Fig. 11(b) is a plot of the modal power flow $\vec{P}_{11}/D\omega_{11}$ in the plate. Significant changes in amplitude and direction of the modal power flow can be observed in and around both of the damage regions. Fig. 11(c) is a plot of the modal power flow using the streamline representation in the damaged plate. The streamlines around the damage regions are discontinued because of the big changes of modal power flow in and around the damage regions.

3.3. Modal power flow in a plate with a small hole

Modal power flow of a thin rectangular plate of size $0.8\times0.6\times0.01\,\mathrm{m}^3$ with a small hole of size $0.01\times0.01\times0.01\,\mathrm{m}^3$ at the center as illustrated in Fig. 12(a) is studied using the commercial finite element software, *Patran*. There are 4799 elements in the finite element model. Vibration mode shapes are calculated by using *Patran*. The mode shape data is exported as text file and then imported in *Matlab* for the calculations

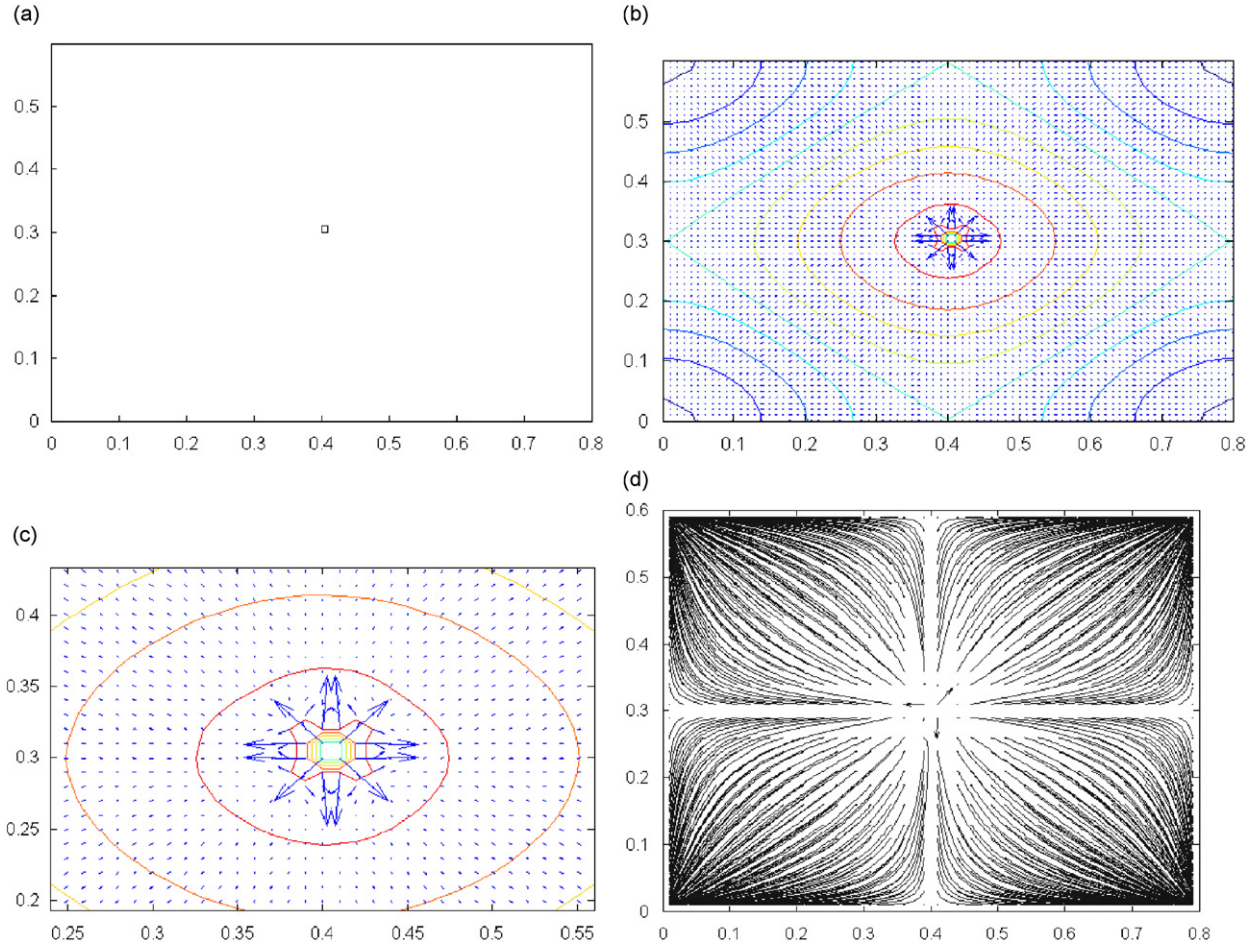

Fig. 12. (a) A simply supported plate with a small hole at the center, (b) modal power flow $\vec{P}_{11}(x,y)/D\omega_{11}$ (illustrated by the arrows) and contours of $T_{11\_max}-V_{11\_max}$, (c) modal power flow $\vec{P}_{11}(x,y)/D\omega_{11}$ around the hole and contours of $T_{11\_max}-V_{11\_max}$, and (d) streamline representation of the modal power flow $\vec{P}_{11}(x,y)/D\omega_{11}$ of the simply supported rectangular plate.

of the reactive power flow distribution following Eqs. (30) and (31). Fig. 12(b) is a plot of the modal power flow $\vec{P}_{11}/D\omega_{11}$ and Fig. 12(c) is a close up of the modal power flow around the hole. Very large variation of the power flow vectors is observed around the hole. Fig. 12(d) is the streamline representation of the modal power flow in the damaged plate. The streamlines around the damage region is discontinued because of the big changes of modal power flow around the damage region.

4. Conclusions

Modal energy distributions and modal power flow in a damaged plate are studied, with the objective to demonstrate the capacity of modal power flow as a damage indicator. It is shown that the local time-averaged energy ($T_{\max}+U_{\max}$) increases at the damage region, hence the damage region behaves as an energy trap. Energy flowing in and out of the damage region to the surrounding regions may be increased or decreased depending on the location of the damage.

The capability for damage location identification for plate-like structures using modal reactive power flow is then demonstrated. Compared with the conventional damage indicators such as the change of strain mode shape of the plate, the proposed one is new and found to be more sensitive to the reduction of plate stiffness than the strain mode shape.

Moreover, compared with the damage identification techniques based on the determination of the active power flow in a damaged plate, the proposed method only requires information of a vibration mode shape of the structure and it is easier to apply in practice. Two common types of damage are tested for identification. The first type features a region of reduced stiffness in the plate while the other type exhibits a small hole in the plate. Numerical tests show that the proposed method is effective for both types of damage. Experimental study and validation will be carried out and reported in the future.

References

[1] F.K. Chang, *Structural Health Monitoring: Current Status and Perspectives*, Technomic Publishing, Lancaster, PA, 1997.
[2] A. Alvandi, C. Cremona, Assessment of vibration-based damage identification techniques, *Journal of Sound and Vibration* 292 (2006) 179–202.
[3] Y. Zou, L. Tong, G.P. Steven, Vibration-based model-dependent damage (delamination) identification and health monitoring for composite structures—a review, *Journal of Sound and Vibration* 230 (2000) 357–378.
[4] H.P. Chen, N. Bicanic, Assessment of damage in continuum structures based on incomplete modal information, *Computers and Structures* 74 (2000) 559–570.
[5] Y.Y. Li, L. Cheng, L.H. Yam, W.O. Wong, Identification of damage locations for plate-like structures using damage sensitive indices: strain modal approach, *Computers & Structures* 80 (2002) 1881–1894.
[6] Z.Y. Shi, S.S. Law, L.M. Zhang, Structural damage localization from modal strain energy change, *Journal of Sound and Vibration* 218 (1998) 825–844.
[7] P. Cornwell, S.W. Doebling, C.R. Farrar, Application of the strain energy damage detection method to plate-like structures, *Journal of Sound and Vibration* 224 (1999) 359–374.
[8] N.K. Mandal, S. Biswas, Vibration power flow: a critical review, *The Shock and Vibration Digest* 37 (2005) 3–11.
[9] T.Y. Li, W.H. Zhang, T.G. Liu, Vibrational power flow analysis of damaged beam structures, *Journal of Sound and Vibration* 242 (2001) 59–68.
[10] M.S. Khun, H.P. Lee, S.P. Lim, Structural intensity in plates with multiple discrete and distributed spring-dashpot systems, *Journal of Sound and Vibration* 276 (2004) 627–648.
[11] H.P. Lee, S.P. Lim, M.S. Khun, Diversion of energy flow near crack tips of a vibrating plate using the structural intensity technique, *Journal of Sound and Vibration* 296 (2006) 602–622.
[12] L. Gavric, G. Pavic, A finite element method for computation of structural intensity by the normal mode approach, *Journal of Sound and Vibration* 164 (1993) 29–43.
[13] M.T. Whalen, The behavior of higher order mode shape derivatives in damaged, beam-like structures, *Journal of Sound and Vibration* 309 (2008) 426–464.
[14] D.J. Ewins, *Modal testing: Theory, Practice and Application*, Research Studies Press, Baldock, England, 2000.
[15] W.O. Wong, The effects of distributed mass loading on plate vibration behaviour, *Journal of Sound and Vibration* 252 (2002) 577–583.
[16] Z.S. Liu, H.P. Lee, C. Lu, Structural intensity study of plates under low-velocity impact, *International Journal of Impact Engineering* 31 (2005) 957–975.
[17] X.D. Xu, H.P. Lee, C. Lu, J.Y. Guo, Streamline representation for structural intensity fields, *Journal of Sound and Vibration* 280 (2005) 449–454.